HHS Public Access

Author manuscript

Sci Transl Med. Author manuscript; available in PMC 2020 October 08.

Published in final edited form as:

Sci Transl Med. 2020 April 08; 12(538): . doi:10.1126/scitranslmed.aax5104.

IL-6 Blockade Reverses Bone Marrow Failure Induced by Human Acute Myeloid Leukemia

Tian Yi Zhang[1,2,3], **Ritika Dutta**[1,2], **Brooks Benard**[4], **Feifei Zhao**[1,2,3], **Raymond Yin**[1,2,3], **Ravindra Majeti**[1,2,3,*]

[1]Department of Medicine, Division of Hematology, Stanford University, Stanford, California, 94305, USA

[2]Stanford School of Medicine, Stanford, California, 94305, USA

[3]Department of Medicine, Division of Hematology, Cancer Institute, and Institute for Stem Cell Biology and Regenerative Medicine, Stanford University, Stanford, California, 94305, USA

[4]Cancer Biology Program, Stanford University School of Medicine, Stanford, California, 94305, USA

Abstract

Most patients with acute myeloid leukemia (AML) die from complications arising from cytopenias resulting from bone marrow (BM) failure. The common presumption among physicians is that AML-induced BM failure is primarily due to overcrowding, yet BM failure is observed even with low burden of disease. Here, we use large clinical data sets to show the lack of correlation between BM blast burden and degree of cytopenias at the time of diagnosis. We develop a splenectomized xenograft model to demonstrate that transplantation of human primary AML into immunocompromised mice recapitulates the human disease course by induction of BM failure via depletion of mouse hematopoietic stem and progenitor populations. Using unbiased approaches, we show that AML-elaborated IL-6 acts to block erythroid differentiation at the proerythroblast stage and that blocking antibodies against human IL-6 can improve AML-induced anemia and prolong overall survival, suggesting a potential therapeutic approach.

One Sentence Summary

Acute myeloid leukemia inhibits normal erythroid differentiation through paracrine effects of IL-6.

*To whom correspondence should be addressed: rmajeti@stanford.edu.

Author contributions: T.Y.Z. designed and conducted experiments, analyzed data, and wrote the manuscript. R.D. conducted experiments, helped analyze data and edited the manuscript. F.Z. and R.Y. conducted experiments. B.B. analyzed data. R.M. provided intellectual support and provided funding.

Competing interests: R.M. is a founder, consultant, equity holder, and serves on the Board of Directors of Forty Seven Inc. The other authors report no competing interests and have no paid or unpaid consultancy to report. No patents were filed as the result of this work.

Data and materials availability: All data are available in the main text or the supplementary materials. RNA-Seq data have been deposited in the Gene Expression Omnibus (accession number GSE128910).

Introduction

AML)is an aggressive blood cancer caused by uncontrolled proliferation and accumulation of abnormal myeloid progenitors in the BM and/or peripheral blood (PB) (1). Progressive BM failure is a hallmark of the AML disease course, resulting in decreased production of white blood cells, red blood cells, and/or platelets that lead to high rates of morbidity and mortality (2). In fact, the vast majority of AML patients eventually become transfusion dependent (3). Although red blood cell (RBC) transfusions can help alleviate symptoms of severe fatigue, shortness of breath, and increased cardiac demand, the need for frequent blood draws and long periods of time spent in transfusion centers decrease quality of life. Therefore, identification of targetable factor(s) or pathway(s) that mediate progressive BM failure in AML has the potential for major clinical impact.

Notably, normal hematopoiesis is restored in AML patients who achieve remission, suggesting the presence of a reversible factor or process which drives AML-associated BM failure. Normal blood production results from differentiation of hematopoietic cells from hematopoietic stem and progenitor cells (HSPCs) that reside in the BM (4). This occurs via a highly ordered, multi-step process under tight control of a complex network of intrinsic factors and microenvironmental cues collectively termed the BM niche. Niche factors known to regulate normal hematopoiesis include integrins, cytokines, chemokines, and constituents of the extracellular matrix (5).

Conventional clinical teaching holds that AML-associated BM failure results from the physical crowding of the BM niche by leukemic blasts. However, many AML patients with low leukemic burden (20–30%) and incomplete involvement of the BM compartment exhibit clinical signs of BM failure. These observations suggest that additional mechanisms must be involved in AML-induced BM failure, particularly in patients with incomplete marrow involvement. A number of studies have investigated the effects of AML on normal progenitors and the niche, implicating production of AML-secreted factors as potential mechanisms driving niche dysfunction (6–8). AML cells have been shown to scavenge critical niche factors, such as thrombopoietin (TPO), and cause differentiation arrest of residual HSCs (9). AML blasts can produce inflammatory cytokines including granulocyte-macrophage colony stimulating factor (GM-CSF), interleukin 1 beta (IL-1β), tumor necrosis factor alpha (TNFα), interleukin 6 (IL-6), C-X-C motif chemokine 12 (CXCL2), and C-C motif chemokine ligand 3 (CCL3) which decrease colony-forming potential of normal $CD34^+$ cells and induce endosteal endothelial remodeling and progenitor depletion (10–15).

Studying the mechanisms behind AML-induced BM failure has been hindered by the lack of a model which recapitulates the human disease course. Here, we describe a primary human AML xenograft model that accurately recapitulates AML-induced BM failure resulting in shortened overall survival. Notably, BM failure was observed with 10–70% BM leukemic involvement, indicating that overcrowding could not be the sole mechanism. Using this model, we observed profound depletion of HSPCs, with a particular block in erythroid differentiation, resulting in progressive anemia. Proteomic and transcriptomic studies determined that this effect was mediated by paracrine secretion of IL-6, whose effects could

be reversed with a clinically approved anti-IL-6 blocking antibody that improved overall survival in the xenograft model.

Results

The severity of cytopenias in AML patients is independent of disease burden

A common presumption among physicians is that AML-induced BM failure results from overcrowding of the BM space by AML blasts, suggesting spatial crowding plays a key role in suppressing normal hematopoiesis. While this may be true in cases where the BM is effaced with leukemic blasts, BM failure is observed across the spectrum of disease burden down to 20% marrow involvement (2). We hypothesized that if spatial crowding is the primary mechanism causing AML-induced BM failure, then the degree of marrow crowding should inversely correlate with the severity of cytopenias. To test this, we examined clinical data from a cohort of 293 patients diagnosed with AML at Stanford between 2011–2014 (table S1). Using BM blast percentage as an estimate of disease burden, no correlation was found between the BM blast percentage at diagnosis and the hemoglobin concentration, platelet count, absolute neutrophil count, or absolute lymphocyte count (Fig. 1A–D). Additional analysis of a publicly available dataset of more than 1300 patients also demonstrated that PB blast percentage and mutation burden, as indicated by variant allele frequencies (VAFs), did not correlate with the severity of cytopenias (table S2 and fig. S1–S2) (16). These results indicate that AML leukemic burden and crowding of the BM space are not the primary drivers of AML-induced BM failure.

Splenectomized human AML xenograft mice die of BM failure

Human AML can be studied in vivo through xenotransplantation into immunodeficient mice, particularly the NOD/SCID/IL2R-gamma null strain (NSG) (17, 18). We generated human AML xenografts in NSG mice conditioned with sublethal irradiation followed by intravenous injection of three patient-derived AML samples (NSG-PDX mice). These mice were followed for the development of cytopenias by serial assessment of complete blood counts (CBCs) and AML engraftment by femoral aspirates by flow cytometry (Fig. 2A and fig. S3). Surprisingly, NSG-PDX mice exhibited only mild cytopenias and no signs of BM failure at 12 weeks post-transplantation even with BM leukemic engraftment greater than 60% (Fig. 2B–C and fig. S4A–B). Necropsy analysis of these mice indicated that NSG-PDX mice consistently developed splenomegaly compared to irradiation-only control NSG mice, often as early as 6–8 weeks post-transplantation (Fig. 2D). Histological sections of the spleen from NSG-PDX mice showed a dramatic increase in the number of megakaryocytes and expansion of the red pulp, indicating development of extensive extramedullary hematopoiesis (EMH) (Fig. 2E) (19). Thus, we hypothesized that splenic EMH compensates for AML-induced suppression of BM hematopoiesis in NSG-PDX models, thereby preventing development of cytopenias and early mortality as seen in AML patients.

To test this hypothesis, we developed a xenotransplantation approach in which NSG mice underwent surgical splenectomy or a sham procedure with all steps of the surgery except for removal of the spleen. After recovery from the procedure, both sham-operated (NSG^{sham}) and splenectomized (NSG^{spln-}) mice were sublethally irradiated and transplanted with

primary human AML blasts by intravenous injection (NSG^{sham}-PDX and NSG^{spln-}-PDX). A separate group of sublethally irradiated NSG^{spln-} mice were transplanted with normal human cord blood-derived CD34^{+} progenitors (NSG^{spln-}-CB-CD34^{+}) as additional controls (Fig. 2F and fig. S5) (20). NSG^{sham}-PDX mice generated with 10 well-characterized primary AML samples (table S3) exhibited normal concentrations of hemoglobin at 8 weeks post-transplantation (Fig. S6A). In contrast, NSG^{spln-}-PDX mice engrafted with the same primary AML samples consistently developed pancytopenia (Fig. 2G and fig. S6B–C). Notably, NSG^{spln-}-CB-CD34^{+} mice had normal CBCs (Fig. 2G and fig. S6B–C), indicating an AML-specific effect. Similar to patients with AML, the degree of anemia did not correlate with disease burden under conditions of similar engraftment (Fig. 2H, I). NSG^{spln-}-PDX mice exhibited shortened survival compared to NSG^{sham}-PDX mice engrafted with the same AML sample (Fig. 2J and fig. S7). We investigated the possibility that early mortality of NSG^{spln-}-PDX mice is due to increased leukemic burden but found similar amounts of human AML in the BM, PB, and/or other vital organs (fig. S8A–C). These findings demonstrate that NSG^{spln-}-PDX mice develop pancytopenia due to AML-induced BM failure, resulting in early mortality that recapitulates human disease.

Normal mouse hematopoietic progenitor populations are depleted in the presence of human AML

AML-induced BM failure can occur due to hematopoietic progenitor suppression caused by increased apoptosis/cell death, differentiation arrest, displacement from the BM niche, or any combination of these factors. To differentiate among these possibilities, we enumerated HSPCs from NSG^{spln-}-PDX mice by flow cytometry using established markers (fig. S9 and Fig. 3A) (21). All progenitor populations were reduced in NSG^{spln-}-PDX mice compared to NSG^{spln-}-CB-CD34^{+} mice (Fig. 3B–F). The reduction in HSPCs did not correlate with BM engraftment at week 8 post-transplantation (Fig. 3G–K). The rates of apoptosis/cell death in HSPCs were similar between NSG^{spln-}-PDX and NSG^{spln-}-CB-CD34^{+} mice (fig. S10A). Additionally, HSPCs were rarely detected in the peripheral circulation of NSG^{spln-}-PDX mice, suggesting that displacement of progenitors from the BM niche was not a major contributing factor (fig. S10B). Consistent with EMH compensating for BM failure, HSPCs were similarly depleted in the BM of NSG^{sham}-PDX mice (fig. S11).

We further examined erythroid progenitors, and found similar numbers of proerythroblasts between NSG^{spln-}-PDX and NSG^{spln-}-CB-CD34^{+}mice (Fig. 4A). Contrastingly, all other erythroid progenitors were reduced in NSG^{spln-}-PDX mice (Fig. 4B–E). As with anemia, depletion of erythroid progenitors did not correlate with AML engraftment (Fig. 4F–I). Similar to other HSPCs, we found no evidence that increased apoptosis/cell death or peripheral displacement from the BM niche contributed to erythroid progenitor depletion beyond the proerythroblast stage (fig. S12). These results suggest that AML blasts may cause anemia by imparting a differentiation block on proerythroblasts.

Human AML suppresses normal hematopoiesis via a paracrine factor(s)

To examine the possibility that AML can suppress normal hematopoiesis through the paracrine effects, we conducted mouse progenitor colony-forming assays in methylcellulose supplemented with CM from in vitro cultured flow-purified primary AML blasts (AML-

CM) and CB-CD34$^+$ cells (CB-CD34$^+$-CM) (Fig. 5A and fig. S13–14). Primary AML blasts exhibited viability >85% in vitro (fig. S15A), which was improved by flow-sorting on PI$^-$ AnnexinV$^-$CD33$^+$CD45^{low}CD3$^-$ blasts (fig. S15B). The numbers of mouse BFU-E and CFU-GEMM were decreased in the presence of AML-CM relative to CB-CD34$^+$-CM (Fig. 5B, C and table S4). Similar experiments were conducted with human CB-CD34$^+$ cells and demonstrated that AML-CM suppressed human BFU-E (Fig. 5D, E and table S5). AML-CM from some samples (SU266 and SU353) inhibited the generation of human CD34$^+$ colonies of any type. Notably, AML-CM increased the number of human CFU-G and CFU-M, but not mouse CFU-G or CFU-M (Fig. 5D–E and tables S3 and S4).

Next, we used a co-culture system to further study the effects of AML blasts on erythroid differentiation by culturing CB-CD34$^+$ cells (top) and human AML blasts (bottom) across a semipermeable transwell membrane in the presence of established erythroid differentiation factors IL-3, SCF, and EPO (see Fig. 5F) (22, 23). Erythroid differentiation was assessed over 3 weeks using well-established markers CD71 and CD235a/GPA to define proerythroblasts, normoblasts, and reticulocytes (24). The presence of AML blasts decreased the percentage and absolute number of normoblasts in our erythroid differentiation culture (Fig. 5F, G and fig. S16A). To investigate the possibility that AML blasts inhibited differentiation of erythroid progenitors by modulating cell cycle status or by causing increased cell death, we determined 5-ethynyl-2'-deoxyuridine (EDU) uptake and cell viability. A similar percentage of CB-CD34$^+$ cells exhibited EDU uptake in control and AML co-cultures (fig. S16B). In addition, no consistent differences in CB-CD34$^+$ cell death were observed between control and AML co-cultures (fig. S16C). Thus, human AML blasts elaborate a secreted factor(s) that suppresses erythroid differentiation of normal mouse and human progenitors.

IL-6 is differentially upregulated and secreted by AML blasts

To identify AML-elaborated paracrine factors that can suppress erythroid differentiation, we performed RNA-Seq on flow-purified blasts from primary patient samples (n=7) and flow-purified CB-CD34$^+$ cells (n=4) after 72-hour culture. Differentially upregulated genes in AML blasts compared to CB-CD34$^+$ cells were enriched for signatures involved in defense/immune responses, inflammatory mediators, and cytokine signaling and response pathways (Fig. 6A, fig. S17A,B), and included 52 genes involved in cytokine signaling upregulated by at least 8 fold ($p < 0.00005$) in AML blasts (Fig. 6B). In parallel, we conducted Luminex multiplex protein assays to identify secreted proteins from primary AML samples used previously. These assays identified 12 factors produced in increased amounts (>2 fold) by flow-sorted AML blasts (Fig. 6C), and 7 factors that were increased (>2 fold) in the BM of NSG^{spln-}-PDX mice engrafted with SU540 and SU555 compared to NSG^{spln-}CB-CD34$^+$ mice (Fig. 6D). Intersecting the results of all three assays identified IL-6 as a secreted factor upregulated in human primary AML blasts both in vitro and in vivo (Fig. 6E, F).

Human AML suppresses erythroid differentiation and causes anemia via paracrine effects of IL-6

To investigate the role of IL-6 in AML-mediated erythroid differentiation block, we used a neutralizing antibody specific for human IL-6 (hIL-6) to block its activity in our in vitro

assays (Fig.7). AML-CM again decreased the number of BFU-E colonies generated by normal CB-CD34$^+$ progenitors (Fig. 7A). However, this effect was completely reversed in the presence of the neutralizing hIL-6 antibody. Furthermore, addition of the same antibody to our erythroid differentiation co-culture assay partially reversed the differentiation block of normal CB-CD34$^+$ progenitors from the proerythroblast to normoblast stage (Fig. 7B). In contrast, the addition of recombinant hIL-6 to normal CB-CD34$^+$ erythroid differentiation cultures decreased the absolute number of normoblasts (fig. S18).

Siltuximab is an FDA-approved IL-6 neutralizing antibody treatment for idiopathic multicentric Castleman's disease (25). We used siltuximab in NSG^{spln-}-PDX mice to investigate the role of human AML-secreted IL-6 in AML-induced BM failure. Siltuximab or control antibody (20 mg/kg) was administered to NSG^{spln-}-PDX mice transplanted with four primary human AML samples (SU540, SU575, SU555, and SU351) via intraperitoneal injection beginning on day 3 after transplantation (Fig. 7C). CBCs were obtained every two weeks to determine the degree of anemia and disease burden was assessed at 6–8 weeks. Strikingly, siltuximab treatment increased hemoglobin concentrations as early as 2 weeks into treatment in NSG^{spln-}-PDX mice under conditions of similar BM engraftment (Fig. 7D–G and fig. S19A–D). Siltuximab treatment increased overall survival (Fig. 7H–K). This was also associated with an increased in absolute numbers of normoblasts in siltuximab treated NSG^{spln-}-PDX mice (Fig. 7L–M).

We investigated the possibility that the IL-6 blockade decreased disease burden but found no differences in the percentages of AML blasts in PB or vital organs with treatment (fig. S19E, F, S20). We found that siltuximab treatment initiated later in the disease course (d21) also improved concentrations of hemoglobin and overall survival, although to a lesser extend (fig. S21A–C, Fig. 7N).

Finally, given that IL-6 has a well-described role in anemia of inflammation/anemia of chronic disease through upregulation of hepcidin (26), we measured serum hepcidin in NSG^{spln-}-AML and NSG^{spln-}-CB-CD34$^+$ mice and found no differences in serum hepcidin concentrations (Fig. 7O). Because NSG^{spln-}-CB-CD34$^+$ mice did not develop anemia, it is unlikely that AML-derived IL-6 causes anemia via hepcidin effects. We did not find IL-1β or CCL3 to be consistently produced by human AML blasts in culture or in vivo in NSG-PDX mice as previously reported (fig. S22) (11).

Discussion

Marked morbidity and mortality in AML result from the clinical syndrome of BM failure which has historically been presumed to be related to overcrowding of BM space. Here, we challenge this traditional view by (1) showing clinical evidence that there is a lack of correlation between AML BM blast burden and the degree of cytopenia in patients with AML at the time of diagnosis, (2) establishing a splenectomized NSG xenograft model demonstrating that AML, but not CB, engraftment induces BM failure in vivo, (3) demonstrating that AML blasts can block erythroid differentiation at the proerythroblast stage by elaboration of IL-6, (4) providing evidence that blocking anti-human IL-6

antibodies can reverse these effects in vitro and improve BM failure and overall survival in vivo.

The pathologic diagnosis of AML requires greater than 20% BM blasts, and patients are observed along the entire spectrum from 20–100% (2). Indeed, in patients with very high burdens of disease (>70%), it is likely that there are additional mechanisms of BM failure compared to those with low burden. This possibility was suggested by studies using conventional AML xenograft models in which differentiation arrest of HSCs and subsequent progenitor depletion was found only late in the disease course, when engraftment exceeded 70% (27). In contrast, low amounts of AML burden (<40%) did not cause critical depletion of mouse progenitors in the BM (27). High burdens of disease can also impact the BM microenvironment, and destruction of endosteal endothelium was demonstrated with high disease burden using an AML xenograft model (10). The authors found local production of the inflammatory cytokines TNFα and CXCL2 and hypothesized that this contributed to endothelial BM niche dysfunction. These studies suggest that distinct mechanisms are involved in BM failure associated with a high burden of disease, whereas our results demonstrate that profound depletion of mouse progenitors associated with severe anemia and early death occurred at low to moderate amounts (20–40%) of disease in splenectomized AML xenografts, consistent with a separate, paracrine-mediated mechanism resulting in BM failure.

Our transcriptome and protein array results illustrate a common inflammatory response in primary AML blasts, and inflammatory mediators have recently been implicated in leukemia-mediated niche dysregulation (28). Several studies have examined the role of cytokines and niche factors in AML-induced BM failure (10, 29, 30). In one study, MPL^{high} AML blasts exhibited the ability to scavenge TPO causing HSPC exhaustion (9). Inflammatory cytokine production has also been implicated in AML-induced BM failure (11, 12, 30). Using inhibitors of IL-1β signaling, the authors showed normalization of IL-1β-mediated growth suppression of normal $CD34^+$ cells. In a separate study, increased circulating concentrations of the chemokine CCL3 were found in newly diagnosed AML patients and the plasma of a mouse model of MLL-AF9 AML (13). In this mouse model, there was reduced proliferation of MEPs in vivo and decreased BFU-E formation in the presence of exogenous CCL3 or leukemic BM plasma, which was reversed by CCL3 blockade. This may be due to differences in methodologies and does not rule out a role for these cytokines/chemokines in disruption of normal hematopoiesis by AML blasts (13).

One potential limitation of our studies is the differential cross-species effects of paracrine factors and their cognate receptors (31, 32). In our in vitro assays, for example, AML-CM increased the number of human CFU-G, but its effects on mouse CFU-G were more variable. A similar situation could impact our ability to detect the effects of human AML-elaborated paracrine factors on mouse HSPCs and niche supporting cells through their cognate receptor. Another limitation of the xenograft model is the use of irradiation for priming before transplantation of human AML cells, which can affect mouse HSPC function in addition to effects exerted by human AML. However, we controlled for these effects by comparing NSG^{spln-} mice engrafted with human AML to those engrafted with CB-$CD34^+$ cells.

AML-produced IL-6 has been reported and hypothesized to be an autocrine growth factor (12, 33). High circulating IL-6 concentrations portend a worse prognosis, associated with decreased event-free survival and overall survival in adult and pediatric AML patients (34), and IL-6 drives progression of chronic myelogenous leukemia, multiple myeloma, and multicentric Castleman's disease (MCD) (35–37). We show evidence that siltuximab reverses AML-induced erythroid differentiation blockade and improves the survival of human AML xenografts. Whether siltuximab can decrease transfusion dependence in AML patients and improve their quality of life should be explored in a safety and feasibility study.

Materials and Methods

Study design

The overall objective of our studies was to identify secreted factors from human AML blasts which inhibited the growth and/or function of HSPCs. We used a set of 10 human primary AML samples to screen for paracrine factors that are made in substantial amounts in vitro and cause BM failure and cytopenias in xenograft mice. We used colony-forming assays and erythroid differentiation cultures to identify progenitor dysfunction in vitro. We used at least 3 biological replicates for every assay, and each experiment was performed at least 3 times using technical triplicates wherever applicable. Each mouse experiment included at least 5 mice in each group. All data points collected were included in the analysis of the experiments and no outliers were excluded. No power analysis was performed for the experiments. Randomization and blinding were not applicable to our studies.

Animal care

All mouse experiments were conducted in accordance with a protocol approved by the Institutional Animal Care and Use Committee (Stanford Administrative Panel on Laboratory Animal Care no. 22264) and in adherence with the US National Institutes of Health's Guide for the Care and Use of Laboratory Animals.

Primary human samples

AML and cord blood samples were obtained according to the Administrative Panel on Human Subjects Research Institutional Review Board (IRB) approved protocols (Stanford IRB no. 6453) with informed consent. Cord blood was collected with written informed consent from the mothers at delivery at the Lucile Packard Children's Hospital (Stanford IRB no. 33818) or purchased from the New York Blood Center (NYBC).

Public data analysis

Using publicly available data from Papaemmanuil et al., (16) we performed linear regression between the PB or BM blast percentages and PB counts for 1,376 adult (18 years or older) patients with AML. For estimation of AML disease burden using VAF of pre-leukemic mutations (ASXL1, IDH1, IDH2, DNMT3A) and somatic mutations (TET2, NPM1, FLT3-ITD, RUNX1, TP53) in AML, we performed linear regression using VAF and PB counts. Statistical analysis was performed using Pearson's correlation coefficient and corresponding p values.

Cell culture

We used multiparametric flow cytometry to identify and sort AML blasts ($CD45^{low}$ $CD33^{mid}CD19^{-}CD3^{-}$) and normal CB-$CD34^{+}$ ($CD34^{+}CD3^{-}CD19^{-}$). Post-sort analysis demonstrated > 98% purity. Sorted cells were cultured in StemSpan (Stem Cell Technologies) supplemented with human recombinant TPO, SCF, and Flt3-L (all 20 ng/ml, PeproTech) at a density of 5×10^{5}/ml for 72 hours, and supernatant was collected to create a cell-free conditioned medium.

CBC

Blood was obtained by collection of 20 μl of blood from the tail vein using an EDTA-coated capillary tube and analyzed by the HemaTrue Veterinary Hematology Analyzer (Heska).

Histological studies

Spleens were removed and immersed in 4% paraformaldehyde for fixation and kept at 4°C overnight. Femurs were explanted and fixed with paraformaldehyde before decalcification using DECAL (American MasterTech) according to manufacturer's protocol. Samples were processed, embedded in paraffin, and sectioned at 4 μm. Immunohistochemistry (IHC) was performed on a Bond Rx autostainer (Leica Biosystems) with enzyme treatment (1:1000) using standard protocols. Bond Polymer Refine Detection (Leica Biosystems) was used according to manufacturer's protocol. After staining, sections were dehydrated and film cover-slipped using a TissueTek-Prisma and Coverslipper (Sakura). Whole slide scanning (40x) was performed on an Aperio AT2 (Leica Biosystems). For histological evaluation of additional organs in xenografted mice, the heart, liver, lung, and kidneys were explanted, fixed with paraformaldehyde, and embedded in paraffin. 10 μm sections were placed on glass slides, and IHC was performed using anti-human CD45 antibody (D9M8I) and polymer HRP secondary antibody at 1:1000 (VectorLabs).

Progenitor enumeration

The tibia, femur, pelvis, and spine of each animal were isolated to generate a mononuclear cell suspension in 2 mM EDTA/PBS which was stained using human CD45, mouse CD45, and mouse lineage markers (CD3, CD4, CD5, CD7, CD19, CD20, CD14, CD11b, CD11c, NK1.1, B220, Sca-1, c-Kit, CD41, CD34, CD150, CD48, FcRγ, and annexin V). Cells were stained in the dark for 30 minutes at 4°C, washed, resuspended in PI-containing buffer (2% FBS in PBS) and analyzed using a BD FACSAria II. Mouse HSCPs were identified by the following gates: HSC $Lin^{-}Sca\text{-}1^{+}c\text{-}Kit^{+}CD41^{-}CD34^{-}CD150^{+}CD48^{-}$, MPP $Lin^{-}Sca\text{-}1^{+}c\text{-}Kit^{+}CD34^{-}CD150^{-/+}CD48^{+}$, CMP $Lin^{-}Sca\text{-}1^{-}c\text{-}Kit^{+}CD34^{high}CD32/16^{-}$, GMP $Lin^{-}Sca\text{-}1^{-}c\text{-}Kit^{+}CD34^{+}CD32/16^{high}$, MEP $Lin^{-}Sca\text{-}1^{-}c\text{-}Kit^{+}CD34^{-}CD32/16^{-/low}$.

Surgical splenectomy

NSG mice at 8–10 weeks of age were sedated using halothane. During sedation, an incision was made along the left costal margin through the peritoneal membrane. The spleen was visualized and isolated using forceps. The splenic artery and vein were cauterized using electric cautery and the spleen removed. A single suture was used to close the peritoneal membrane, and a surgical clip was placed to juxtapose the edges of the incision site. Sham

operation included all steps as described with the exception of cautery and spleen removal. Animals were monitored daily and surgical clips removed at 7 days.

NSG xenotransplantation

Sex- and age- (8–10 weeks) matched NSG mice were conditioned with a sublethal dose of irradiation (200 rad) 12–24 h before transplantation (Faxitron, X-ray irradiation). Irradiation-conditioned NSG mice were transplanted with either primary AML blasts (10^6) or normal $CD34^+$ HSPCs (10^5) in 100 μl PBS via tail vein injection. For AML, freshly thawed primary AML samples were subjected to T cell depletion using anti-CD3 magnetic beads (Robosep, Stem Cell Technologies).

Assessment of human engraftment

Engraftment was evaluated by BM aspirates were taken from the distal end of the right or left femur using a 29-gauge needle under sedation. To remove red blood cells, ACK lysis was performed (RBC lysis buffer, EBioscience). After RBC lysis, cells were blocked (anti-mouse FcR antibody 1 μg/10^6 cells, 15 min, RT) and stained (30 min, 4°C, in the dark) with fluorochrome-conjugated monoclonal antibodies with specificity for human CD45-V450 (dilution 1:25; clone H130), CD19-APC (dilution 1:25; clone HIB19), CD3-APC-Cy7 (dilution 1:50; clone SK7), CD33-PE (dilution 1:25; clone WM53), mouse CD45.1-PE-Cy5 (dilution: 1:100; clone 30-F11). Uni-lineage engraftment by human cells that were $CD45^+CD33^+CD19^-CD20^-CD3^-$ was considered successful engraftment by human AML. Bi-lineage engraftment by human cells that were $CD45^+CD33^+CD19^-CD3^-$ or $CD45^+CD33^-CD19^+CD3^-$ was considered successful engraftment by human normal $CD34^+$ HSPCs.

Colony-forming assay

Both mouse and human colony-forming assays were performed as described (39) and modified with the addition of CM from primary AML blasts or CB-$CD34^+$ cells. 2500–5000 CB-$CD34^+$ or 10,000 bulk mouse BM cells were added to 4 mL of MethoCult H4434 (human, STEMCELL Technologies) or MethoCult M3434 (murine, STEMCELL Technologies) containing 300μL of CM plated in triplicate in a SmartDish (STEMCELL Technologies). Plates were incubated at 37°C and 5% CO_2. The number of colonies in each sample was scored between 10–14 days by morphologic assessment to determine the number of BFU-E, CFU-GEMM, CFU-M, CFU-G, and CFU-GM colonies. For IL-6 neutralization experiments, antibody specific for human IL-6 (1 μg/ml, ThermoFisher) or an isotype control antibody (1 μg/ml, ThermoFisher) was added to the methylcellulose along with CM and mixed before addition of cells.

Erythroid differentiation assay

Erythroid differentiation co-cultures were carried out using a 24-well plate and semipermeable transwells (0.4 μM pores, Sigma-Aldrich). Flow-purified AML blasts were plated (5×10^5/ml) on the bottom of the transwell where indicated and cultured for 72 hours in StemSpan supplemented with Erythroid Expansion Supplement (StemCell Technologies). After 72 hours, normal CB-$CD34^+$ cells (10^4) were added to the top to allow for erythroid differentiation. A 50 μl aliquot was removed from the top of the transwell at various time

points to quantitate erythroid progenitors immunophenotypically using CD71 and CD235a/GPA. For IL-6 blocking experiments, neutralizing antibodies for human IL-6 and an isotype control antibody (both 1 μg /ml, ThermoFisher) were added at the beginning of the culture and replaced every 72 hours during medium change. For cell cycle analysis, EDU was added to erythroid differentiation cultures for 12 h for incorporation during S/G2 phase of the cell cycle. EDU stain was performed according to manufacturer's instructions (Click-iT EdU Cell Proliferation Kit, ThermoFisher) and analyzed by flow cytometry. EDU-positive cells indicated S/G2 phase of the cell consistent with actively proliferating cells. PI was used to distinguish live/dead cells.

RNA-Sequencing

RNA was isolated using the RNeasy Mini Kit (Qiagen) and sequenced and analyzed by Girihlet. RNA with RIN 9 was reverse transcribed to cDNA and libraries were prepared using 500 ng of total RNA with the TruSeq RNA Sample Preparation Kit v2 (Illumina). mRNA-seq and data analysis cDNA libraries were sequenced on the Illumina NextSeq platform to obtain 80-bp single-end reads. The reads were trimmed, compressed, and mapped to the human genome. In order to compare the expression in different samples, quantile normalization was used. The ratios of expression were then calculated to estimate the log (to base 2) of the fold-change. A regularizer (5) to each value, ensuring that genes with expression around or below 5 would appear to have low fold-change as has been described (38). Data were analyzed using MATLAB 2018a. Differentially expressed genes were determined using a negative binomial model as described previously (39, 40) with the Benjamini-Hochberg (BH) adjustment for p-values (41). P-value threshold was set to 0.00005, and differentially expressed genes were considered at 8-fold change. Gene ontology analysis was performed using the PANTHER Gene Ontology Consortium tool (42, 43).

Multiplex protein array

CM from human AML and BM aspirates from NSG^{spln-}-PDX mice were analyzed by the Stanford Human Immune Monitoring Core using a 62-plex Luminex-based custom assay designed to include 62 human secreted proteins by eBioscience (please see http://iti.stanford.edu/himc/immunoassays.html for a complete list of secreted proteins included in the custom capture panel).

In-vivo IL-6 neutralization with siltuximab

Groups of NSG mice underwent surgical splenectomy as described. After recovery, splenectomized NSG mice were sublethally irradiated (200 rads) and transplanted with 2e6 primary human AML blasts via tail vein injection within 24 hours of receiving conditioning irradiation. CBC was obtained at two-week intervals as described above. At 6 weeks after transplantation, femoral aspirates were performed under sedation to evaluate engraftment. Mice were followed and euthanized when hemoglobin reached 2.5 mg/dL or below. Siltuximab treatment was administered starting on day 3 or day 21 via intraperitoneal injection at 20 mg/kg every three days, which has been shown to effectively neutralize IL-6 function in solid tumor xenograft models (44). Control mice engrafted with AML were treated with control IgG (20 mg/kg).

Statistics

GraphPad Prism 8 was used to perform all statistical analyses with the exception of analysis of large public data sets. Error bars represent SEM. The value of alpha (significance level) was set at 0.05. An unpaired (two-tailed) t test was used to define statistical significance when two groups were compared. One way ANOVA was used to calculate statistical differences when more than two groups were compared. Figure legends note statistical parameters for each experiment. *P < 0.05, **P < 0.01, ***P < 0.001, and ****P < 0.0001.

Supplementary Material

Refer to Web version on PubMed Central for supplementary material.

Acknowledgments

We acknowledge Melissa Stanford for management of our mouse colony and primary human AML tissue bank as part of the Hematology Division Tissue Bank, the Stanford Human Immune Monitoring Core for conducting the Luminex assays, and Patty Lovelace for the Flow Core.

Funding: This work was supported by NIH grants (1R01CA188055 to RM and 1R01HL142637 to RM), the Stanford Ludwig Center Grant for Cancer Stem Cells, and Leukemia and Lymphoma Society Scholar Award to RM. T.Y.Z. is supported by the ASH RTAF award, A.P. Giannini Foundation Fellowship Award, Stanford Cancer Institute Fellowship Award. R.D. is supported by the HHMI Medical Fellowship award and the Stanford School of Medicine MedScholars Program.

References and Notes

1. Döhner H, Estey E, Grimwade D, Tallman MS, Tien H-F, Wei AH, Löwenberg B, Bloomfield CD, Diagnosis and management of AML in adults: 2017 ELN recommendations from an international expert panel, Blood 129, 424–447 (2017). [PubMed: 27895058]
2. Arber DA, Orazi A, Hasserjian R, Thiele J, Borowitz MJ, Le Beau MM, Bloomfield CD, Cazzola M, Vardiman JW, The 2016 revision to the World Health Organization classification of myeloid neoplasms and acute leukemia, Blood 127, 2391–2405 (2016). [PubMed: 27069254]
3. Cannas G, Fattoum J, Raba M, Dolange H, Barday G, François M, Elhamri M, Salles G, Thomas X, Transfusion dependency at diagnosis and transfusion intensity during initial chemotherapy are associated with poorer outcomes in adult acute myeloid leukemia, Ann. Hematol 94, 1797–1806 (2015). [PubMed: 26202609]
4. Morrison SJ, Scadden DT, The bone marrow niche for haematopoietic stem cells, Nature 505, 327–334 (2014). [PubMed: 24429631]
5. Crane GM, Jeffery E, Morrison SJ, Adult haematopoietic stem cell niches, Nat. Rev. Immunol 17, 573–590 (2017). [PubMed: 28604734]
6. Hornick NI, Doron B, Abdelhamed S, Cambronne XA, Chakkaramakkil Verghese S, Kurre P, AML suppresses hematopoiesis by releasing exosomes that contain microRNAs targeting c-MYB, Sci. Signal 9, ra88–ra88 (2016). [PubMed: 27601730]
7. Boyd AL, Reid JC, Sabloff M, Xenocostas A, Collins TJ, Bhatia M, Acute myeloid leukaemia disrupts endogenous myelo-erythropoiesis by compromising the adipocyte bone marrow niche, Nat. Cell Biol 19, 1336–1347 (2017). [PubMed: 29035359]
8. Waclawiczek A, Hamilton A, Rouault-Pierre K, Abarrategi A, Bonnet D, Regulation of human stem and progenitor cells by acute myeloid leukaemia in the human niche, Exp. Hematol 53, S60 (2017).
9. Rauch PJ, Ellegast JM, Widmer CC, Fritsch K, Goede JS, Valk PJM, Lowenberg B, Takizawa H, Manz MG, MPL expression on AML blasts predicts peripheral blood neutropenia and thrombocytopenia, Blood 128, 2253–2257 (2016). [PubMed: 27574191]

10. Duarte D, Hawkins ED, Duffy K, Adams RH, Purton LE, Carlin LM, Lo Celso C, Inhibition of Endosteal Vascular Niche Remodeling Rescues Hematopoietic Stem Cell Loss in AML, Cell Stem Cell 22, 64–77.e6 (2018). [PubMed: 29276143]
11. Carey A, Edwards DK, Eide CA, Newell L, Traer E, Medeiros BC, Pollyea DA, Deininger MW, Collins RH, Tyner JW, Druker BJ, Bagby GC, McWeeney SK, Agarwal A, Identification of Interleukin-1 by Functional Screening as a Key Mediator of Cellular Expansion and Disease Progression in Acute Myeloid Leukemia, Cell Rep. 18, 3204–3218 (2017). [PubMed: 28355571]
12. Delwel R, van Buitenen C, Salem M, Bot F, Gillis S, Kaushansky K, Altrock B, Löwenberg B, Interleukin-1 stimulates proliferation of acute myeloblastic leukemia cells by induction of granulocyte-macrophage colony-stimulating factor release, Blood 74, 586–593 (1989). [PubMed: 2665849]
13. Wang Y, Gao A, Zhao H, Yuan W, Zhang X, Hao S, Cheng T, Leukemia cell infiltration causes defective erythropoiesis partially through MIP-1α/CCL3, Leukemia 30, 1897–1908 (2016). [PubMed: 27109512]
14. Broxmeyer HE, Jacobsen N, Kurland J, Mendelsohn N, Moore AS, In vitro suppression of normal granulocytic stem cells by inhibitory activity derived from human leukemia cells, J. Natl. Cancer Inst 60, 497–511 (1978). [PubMed: 625060]
15. Miller AM, Marmor JB, Page PL, Russell JL, Robinson SH, Unregulated growth of murine leukemic cells and suppression of normal granulocyte growth in diffusion chamber cultures, Blood 47, 737–745 (1976). [PubMed: 1260132]
16. Gerstung M, Papaemmanuil E, Martincorena I, Bullinger L, Döhner K, Schlenk RF, Döhner H, Campbell PJ, Precision oncology for acute myeloid leukemia using a knowledge bank approach, Nat. Genet 49, 332–340 (2017). [PubMed: 28092685]
17. Doulatov S, Notta F, Laurenti E, Dick JE, Hematopoiesis: A Human Perspective, Cell Stem Cell 10, 120–136 (2012). [PubMed: 22305562]
18. Ishikawa F, Yoshida S, Ohara O, Akashi K, Harada M, Shultz LD, Chemotherapy-resistant human AML stem cells home to and engraft within the bone-marrow endosteal region, Nat. Biotechnol 25, 1315–1321 (2007). [PubMed: 17952057]
19. Oda A, Tezuka T, Ueno Y, Hosoda S, Amemiya Y, Notsu C, Kasahara T, Nishiyama C, Goitsuka R, Niche-induced extramedullary hematopoiesis in the spleen is regulated by the transcription factor Tlx1, Sci. Rep 8 (2018), doi:10.1038/s41598-018-26693-x.
20. Majeti R, Park CY, Weissman IL, Identification of a hierarchy of multipotent hematopoietic progenitors in human cord blood, Cell Stem Cell 1, 635–645 (2007). [PubMed: 18371405]
21. Chen JY, Miyanishi M, Wang SK, Yamazaki S, Sinha R, Kao KS, Seita J, Sahoo D, Nakauchi H, Weissman IL, Hoxb5 marks long-term haematopoietic stem cells and reveals a homogenous perivascular niche, Nature 530, 223–227 (2016). [PubMed: 26863982]
22. Broudy VC, Morgan DA, Lin N, Zsebo KM, Jacobsen FW, Papayannopoulou T, Stem cell factor influences the proliferation and erythroid differentiation of the MB-02 human erythroleukemia cell line by binding to a high-affinity c-kit receptor, Blood 82, 436–444 (1993). [PubMed: 7687159]
23. Sato T, Maekawa T, Watanabe S, Tsuji K, Nakahata T, Erythroid progenitors differentiate and mature in response to endogenous erythropoietin, J. Clin. Invest 106, 263–270 (2000). [PubMed: 10903342]
24. Hu J, Liu J, Xue F, Chasis GJA, Taylor N, Mohandas N, An X, Isolation and functional characterization of human erythroblasts at distinct stages: implications for understanding of normal and disordered erythropoiesis in vivo, Blood 121, 3246–3253 (2013). [PubMed: 23422750]
25. Deisseroth A, Ko C-W, Sheth C, Gehrke B, Justice R, Farrell A, Pazdur R, FDA Approval: Siltuximab for the Treatment of Patients with Multicentric Castleman Disease, Clin. Cancer Res. 21, 950–954 (2015). [PubMed: 25601959]
26. Ganz T, Longo DL, Ed. Anemia of Inflammation, N. Engl. J. Med 381, 1148–1157 (2019). [PubMed: 31532961]
27. Miraki-Moud F, Anjos-Afonso F, Hodby KA, Griessinger E, Rosignoli G, Lillington D, Jia L, Agrawal S, Gribben JG, Bonnet D, Taussig DC, Acute myeloid leukemia does not deplete normal hematopoietic stem cells but induces cytopenias by impeding their differentiation, Proc. Natl. Acad. Sci 110, 13576–13581 (2013). [PubMed: 23901108]

28. Hemmati S, Haque T, Gritsman K, Inflammatory Signaling Pathways in Preleukemic and Leukemic Stem Cells, Front. Oncol 7 (2017), doi:10.3389/fonc.2017.00265.
29. Zambetti NA, Touw IP, Kuijpers TW, Kanaar R, van de Loosdrecht AA, Vogl T, Raaijmakers MHGP, Mesenchymal Inflammation Drives Genotoxic Stress in Hematopoietic Stem Cells and Predicts Disease Evolution in Human Pre-leukemia, Cell Stem Cell 19, 613–627 (2016). [PubMed: 27666011]
30. Hérault A, Binnewies M, Leong S, Calero-Nieto FJ, Zhang SY, Kang Y-A, Wang X, Pietras EM, Chu SH, Barry-Holson K, Armstrong S, Göttgens B, Passegué E, Myeloid progenitor cluster formation drives emergency and leukaemic myelopoiesis, Nature 544, 53–58 (2017). [PubMed: 28355185]
31. Mestas J, Hughes CCW, Of Mice and Not Men: Differences between Mouse and Human Immunology, J. Immunol 172, 2731–2738 (2004). [PubMed: 14978070]
32. Willinger T, Rongvaux A, Strowig T, Manz MG, Flavell RA, Improving human hemato-lymphoid-system mice by cytokine knock-in gene replacement, Trends Immunol. 32, 321–327 (2011). [PubMed: 21697012]
33. Hoang T, Levy B, Onetto N, Haman A, Rodriguez-Cimadevilla JC, Tumor necrosis factor alpha stimulates the growth of the clonogenic cells of acute myeloblastic leukemia in synergy with granulocyte/macrophage colony-stimulating factor, J. Exp. Med 170, 15–26 (1989). [PubMed: 2664067]
34. Stevens AM, Miller JM, Munoz JO, Gaikwad AS, Redell MS, Interleukin-6 levels predict event-free survival in pediatric AML and suggest a mechanism of chemotherapy resistance, Blood Adv. 1, 1387–1397 (2017). [PubMed: 29296780]
35. Furukawa M, Ohkawara H, Honma R, Watanabe S, Waguri S, Ikezoe T, Takeishi Y, Autocrine and Paracrine Interactions between Multiple Myeloma Cells and Bone Marrow Stromal Cells by Growth Arrest-specific Gene 6 Cross-talk with Interleukin-6, J. Biol. Chem 292, 4280–4292 (2017). [PubMed: 28154173]
36. Reynaud D, Pietras E, Barry-Holson K, Mir A, Binnewies M, Jeanne M, Sala-Torra O, Radich JP, Passegué E, IL-6 Controls Leukemic Multipotent Progenitor Cell Fate and Contributes to Chronic Myelogenous Leukemia Development, Cancer Cell 20, 661–673 (2011). [PubMed: 22094259]
37. van Rhee F, Voorhees P, Dispenzieri A, Casper C, Oksenhendler E, Fajgenbaum DC, International, evidence-based consensus treatment guidelines for idiopathic multicentric Castleman disease, Blood 132, 2115–2124 (2018). [PubMed: 30181172]
38. Howarth DL, Lindtner C, Vasilkova T, Buettner C, Sadler KC, Mullins MC, Ed. Activating Transcription Factor 6 Is Necessary and Sufficient for Alcoholic Fatty Liver Disease in Zebrafish, PLoS Genet. 10, e1004335 (2014). [PubMed: 24874946]
39. Bioinformatics Toolbox (R2018b): Identifying Differentially Expressed Genes from RNA-Seq Data (2018) (available at https://www.mathworks.com/help/bioinfo/examples/identifying-differentially-expressed-genes-from-rna-seq-data.html).
40. Anders S, Huber W, Differential expression analysis for sequence count data, Genome Biol. 11, R106 (2010). [PubMed: 20979621]
41. Benjamini Y, Hochberg Y, Controlling the False Discovery Rate: A Practical and Powerful Approach to Multiple Testing, J. R. Stat. Soc. Ser. B Methodol 57, 289–300 (1995).
42. Mi H, Dong Q, Muruganujan A, Gaudet P, Lewis S, Thomas PD, PANTHER version 7: improved phylogenetic trees, orthologs and collaboration with the Gene Ontology Consortium, Nucleic Acids Res. 38, D204–D210 (2010). [PubMed: 20015972]
43. Thomas PD, PANTHER: A Library of Protein Families and Subfamilies Indexed by Function, Genome Res. 13, 2129–2141 (2003). [PubMed: 12952881]
44. Guo Y, Nemeth J, O'Brien C, Susa M, Liu X, Zhang Z, Choy E, Mankin H, Hornicek F, Duan Z, Effects of Siltuximab on the IL-6-Induced Signaling Pathway in Ovarian Cancer, Clin. Cancer Res. 16, 5759–5769 (2010). [PubMed: 20699329]
45. Mazumdar C, Shen Y, Xavy S, Zhao F, Thomas AD, Koenig JL, Hong W-J, Chang HY, Majeti R, Leukemia-Associated Cohesin Mutants Dominantly Enforce Stem Cell Programs and Impair Human Hematopoietic Progenitor Differentiation, Cell Stem Cell 17, 675–688 (2015). [PubMed: 26607380]

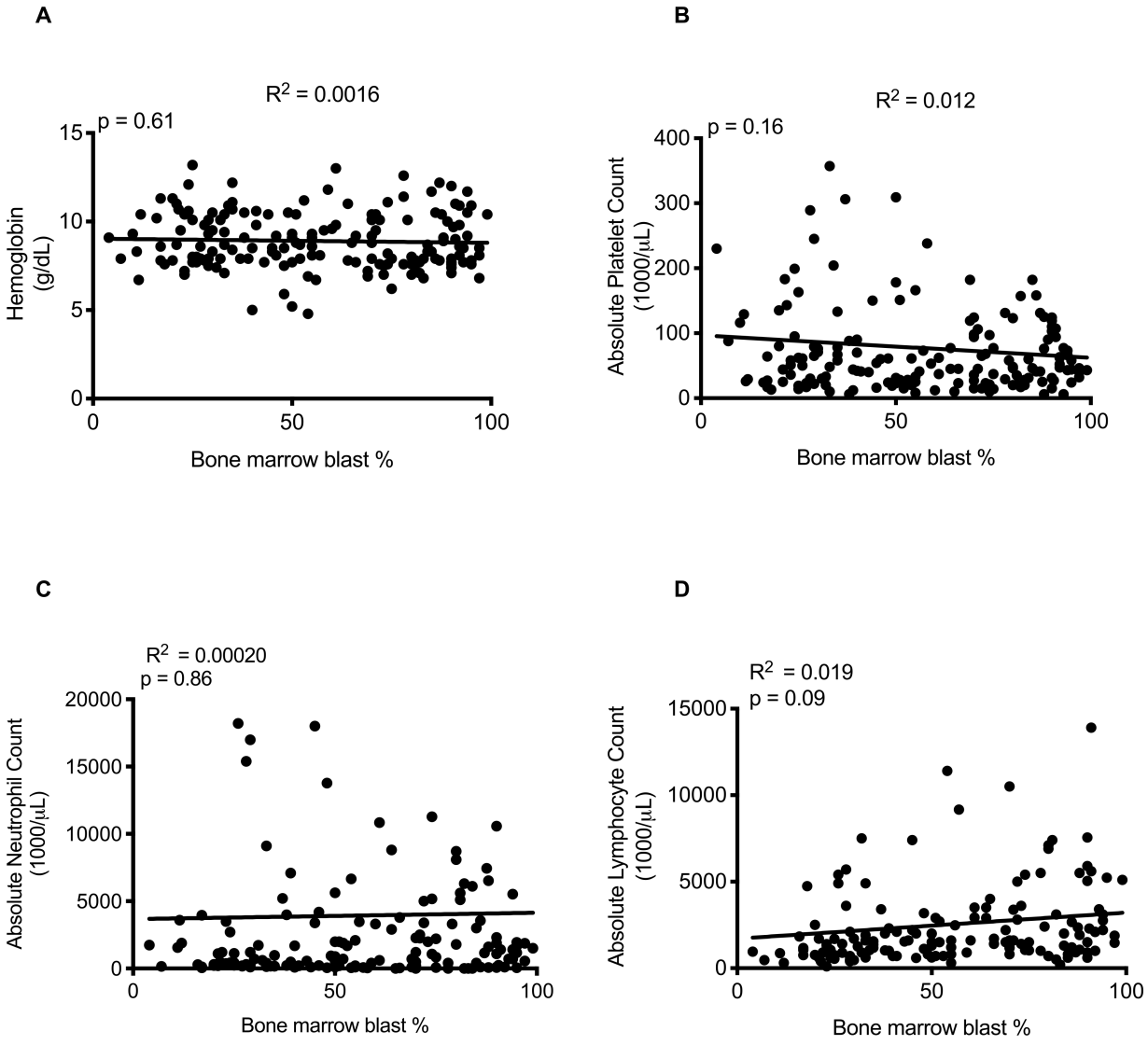

Fig. 1. The severity of cytopenias in AML patients is independent of disease burden

Correlation of (A) hemoglobin (R^2=0.0016, p=0.61), (B) platelet count (R^2=0.012, p=0.16), (C) absolute neutrophil count (R^2=0.00020, p=0.86), and (D) absolute lymphocyte count (R^2=0.019, p=0.09) with BM blast percentage at the time of diagnosis. R^2=Pearson correlation of determination.

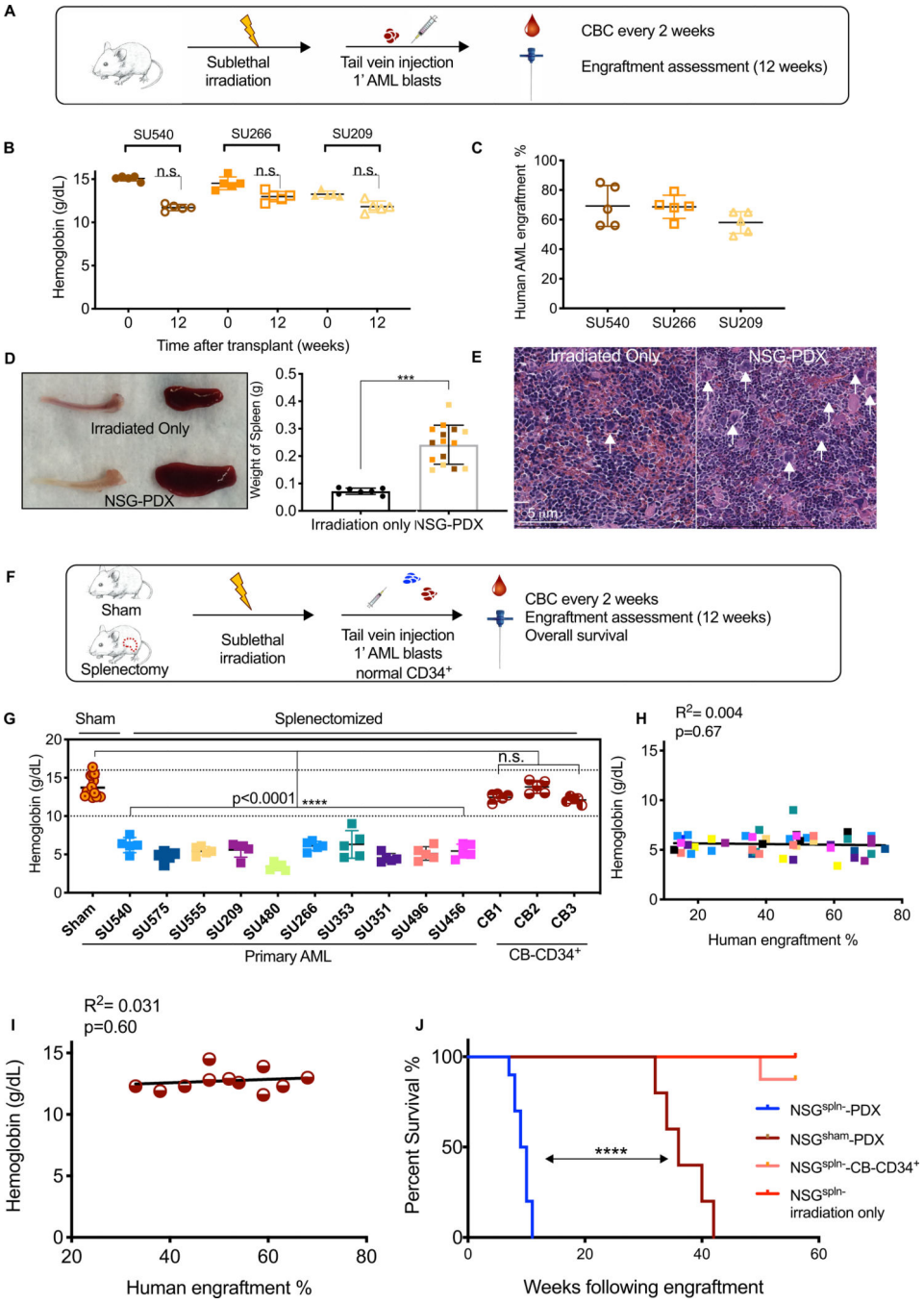

Figure 2. Splenectomized human AML xenograft mice die of BM failure.

(A) Schematic of experimental procedure. (B) Hemoglobin results at 12 weeks are shown. (C) Human AML engraftment at 12 weeks. (D) Representative spleens and tibiae from NSG-PDX and irradiated-only mice are shown on the left. NSG-PDX mice (n=15) demonstrated increased splenic weight (n = 7) ($p < 0.0001$, unpaired t-test). (E) Representative H&E stained spleen sections from NSG-PDX mice demonstrating the presence of increased megakaryocytes (white arrows). Red pulp expansion (red areas) is seen in splenectomized NSG-PDX mice. (F) Schematic of experimental procedure. (G)

Eight weeks after transplantation, hemoglobin was determined in NSG^{spln-}-PDX mice (10 primary AML samples, n = 50 total with 5 mice in each group, $p<0.0001$, 1-way ANOVA) compared to NSG^{sham}-PDX (n=32, 10 independent AML samples) and NSG^{spln-}-CB-CD34^{+} mice (n=15, 3 independent CB) (H) Correlation of hemoglobin and human AML BM engraftment in NSG^{spln-}-PDX mice color-coded to reflect individual AML samples as reported in (D) (n= 46, R^2= 0.02 Pearson correlation determination, p=0.42). (I) Correlation of hemoglobin and BM engraftment in NSG^{spln-}-CB-CD34^{+} mice (n=11, R^2=0.031, p=0.60). (J) Kaplan-Meier survival curve indicating overall survival of NSG^{spln-} irradiated only (n=5, median survival not reached), NSG^{sham}-SU540 (n=5, median survival 36 weeks), NSG^{spln-}-SU540 (n=7, median survival 9.5 weeks), and NSG^{spln-}CB-CD34^{+} (n=5, median survival not reached) engrafted mice. NSG^{spln-}PDX mice have shortened overall survival compared to NSG^{sham-}PDX ($p<0.0001$). n.s. = not significant.

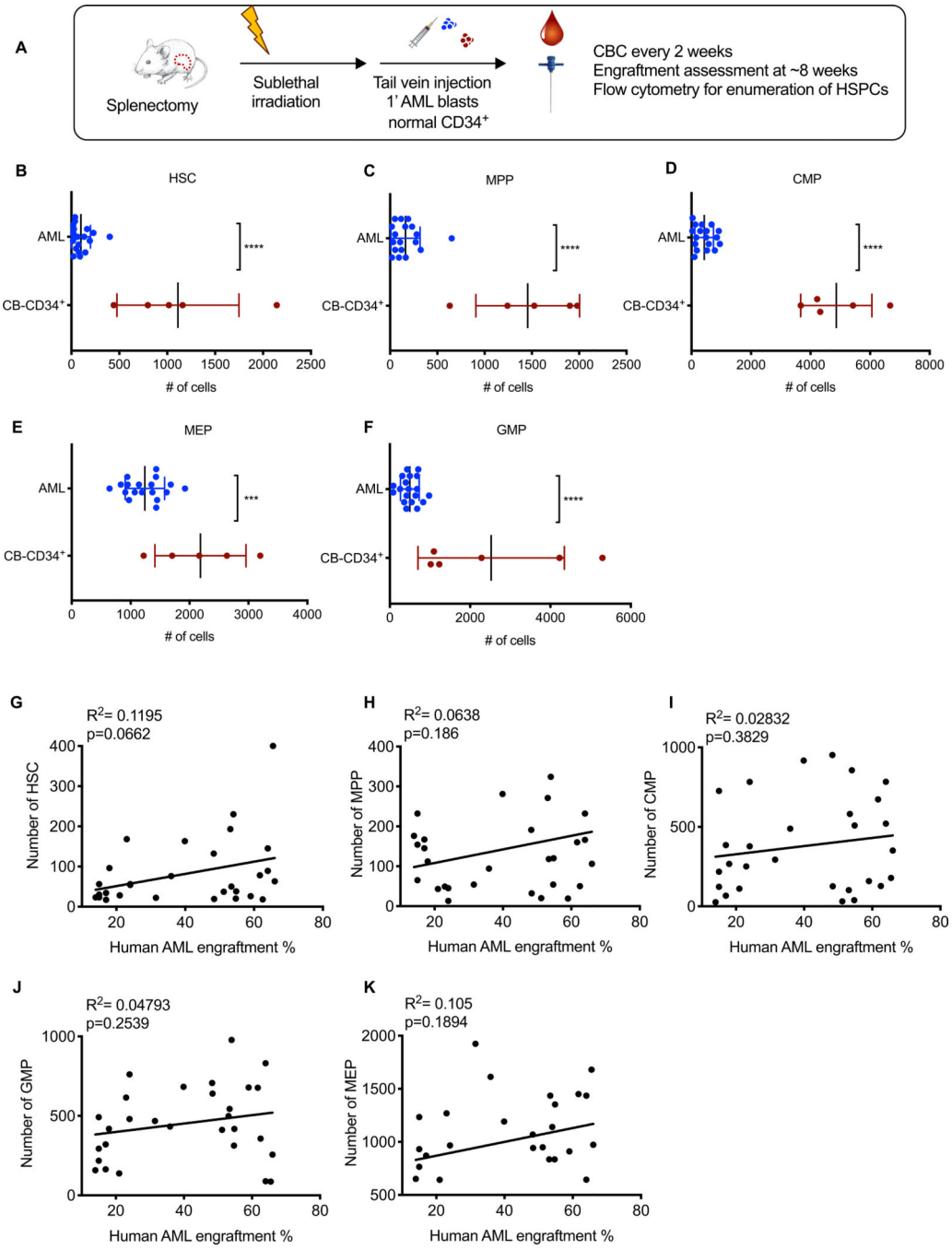

Fig. 3. Normal mouse HSPCs are depleted in the presence of human AML

(A) Schematic of experimental procedure. Absolute numbers of (B) HSC (AML 99.9±23.3 vs CB 1112±285; p<0.0001), (C) MPP (AML 163±36.3 vs CB 1456±245; p<0.0001), (D) CMP (AML 427±74.1 vs CB 4864±534; p<0.0001), (E) MEP (AML 1241±78.8 vs CB 2186±346; p=0.0005), and (F) GMP (AML 498±53.7 vs CB 2525±744; p<0.0001) in NSG^{spln-}-PDX (n=25, engrafted with the same AML samples as in in Fig. 2D, E, absolute numbers represent total numbers per mouse) and NSG^{spln-}-CB-CD34^{+} (n=5, engrafted with the same CB samples as in Fig. 2D, F) mice 8 weeks after transplantation. Pearson's

Correlation between absolute numbers of (G) HSCs, (H) MPP, (I) CMP, (J) GMP, (K) MEPs and BM disease burden as indicated by percent AML engraftment in the BM.

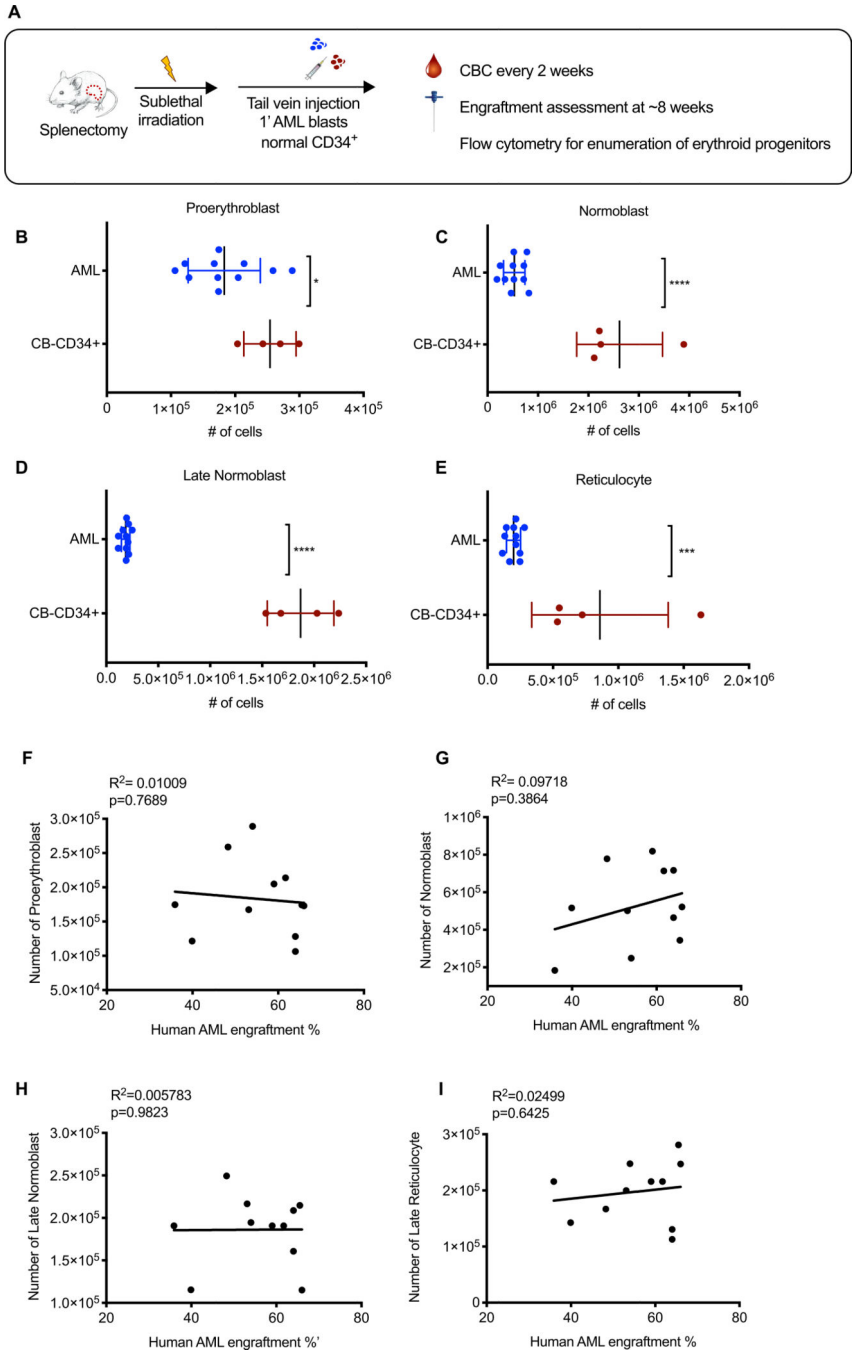

Fig. 4. Human AML blasts impart an erythroid differentiation blockade in vivo.

(A) Schematic of experimental procedure. Absolute numbers of mouse (B) proerythroblasts (AML $1.8\times10^5 \pm 1.7 \times 10^4$ vs CB $2.5\times10^5 \pm 2.0\times10^4$; p=0.034), (C) normoblasts (AML $5.4\times10^5 \pm 6.4\times10^4$ vs CB $2.6\times10^6 \pm 4.3\times10^5$; p<0.0001), (D) late normoblasts (AML $1.86\times10^5 \pm 1.3\times10^4$ vs CB $1.9\times10^6 \pm 1.6\times10^5$; p<0.0001), and (E) reticulocytes (AML $2.0\times10^5 \pm 1.6\times10^4$ vs CB $8.6\times10^5 \pm 2.6\times10^5$; p=0.0007) in the BM of NSG^{spln-}-PDX (engrafted with SU540 (n=6) and SU575 (n=5)) compared to NSG^{spln-}-CB-CD34$^+$ mice (n=4). Absolute numbers represent total numbers per mouse. Pearson's correlation between

absolute numbers of (F) proerythroblasts, (G) normoblasts, (H) late normoblasts, (I) reticulocytes and human AML BM engraftment. All R^2 = Pearson correlation determination.

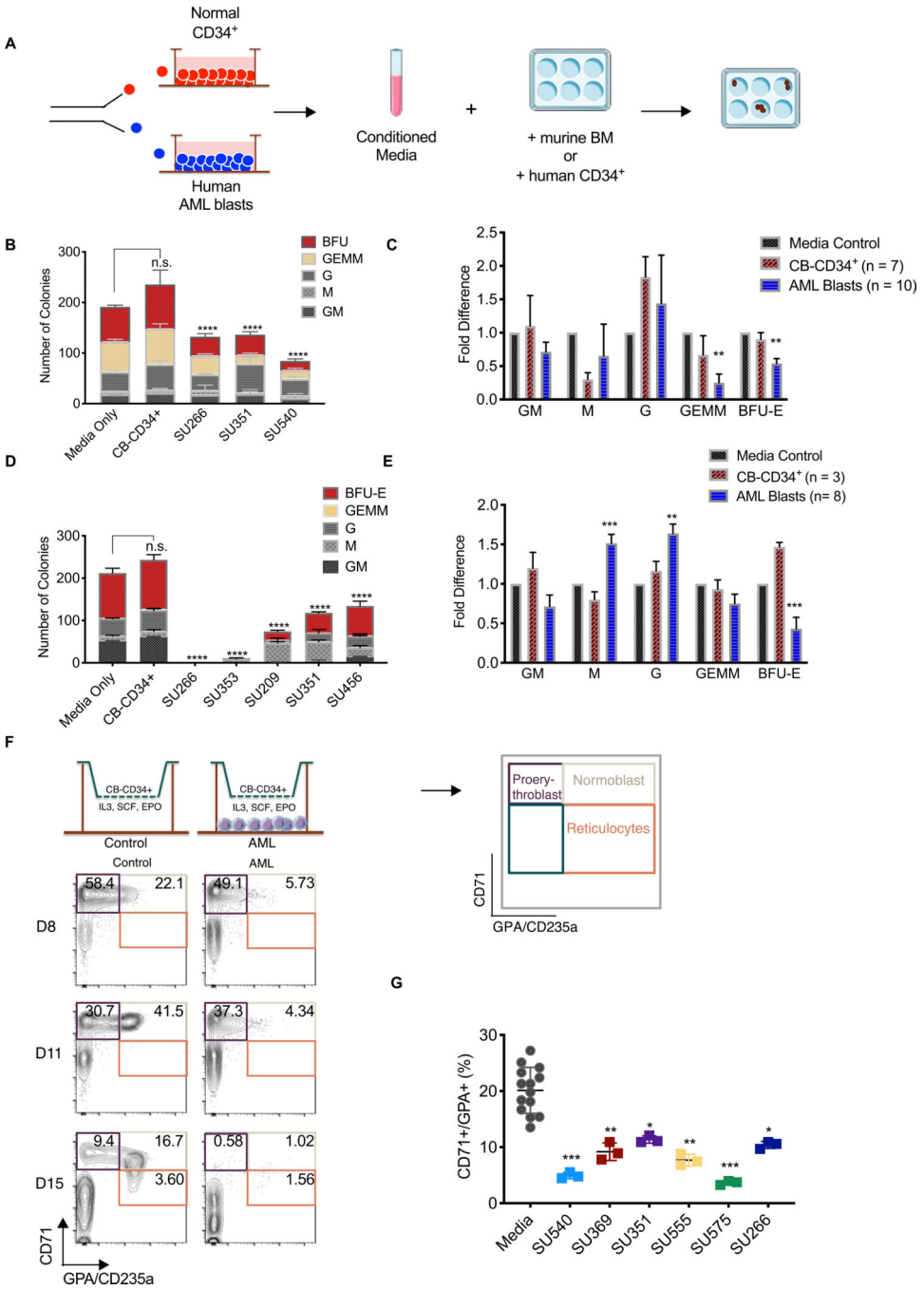

Figure 5. Human AML suppresses normal hematopoiesis via a paracrine factor(s)

(A) Schematic of experimental procedure. (B) Total number and type of colonies formed by mouse BM cells in the presence of CM from CB-CD34$^+$ cells or human AML. $p<0.0001$. (C) Fold change in the number of each colony type generated by normal mouse BM cells in the presence of CM from cultures of purified CB-CD34$^+$ (n=7) or human AML (n=10). For each sample, the number of colonies was normalized to control media. $p<0.01$ (D) Total number and type of colonies formed by human CB-CD34$^+$ cells in the presence of CM from CB-CD34$^+$ cells or human AML. $p<0.0001$ (E) Fold changes in the number of each colony

type generated by normal CB-CD34$^+$ cells in the presence of CM generated from purified CB-CD34$^+$ (n=3) or human AML (n=8). $p<0.001$. (F) Schematic of experimental procedure. At the indicated time points, the top compartment was analyzed for CD71/GPA subpopulations as indicated. Representative CD71/GPA flow cytometry plots at D8, D11, and D15 are shown with percentages of each population indicated from control and AML cultures. (G) The percentage of CD71$^+$/GPA$^+$ normoblasts present on day 6 of the transwell assay in the absence (n=4 with technical triplicates) or presence (n=6 with technical triplicates) of purified AML blasts.

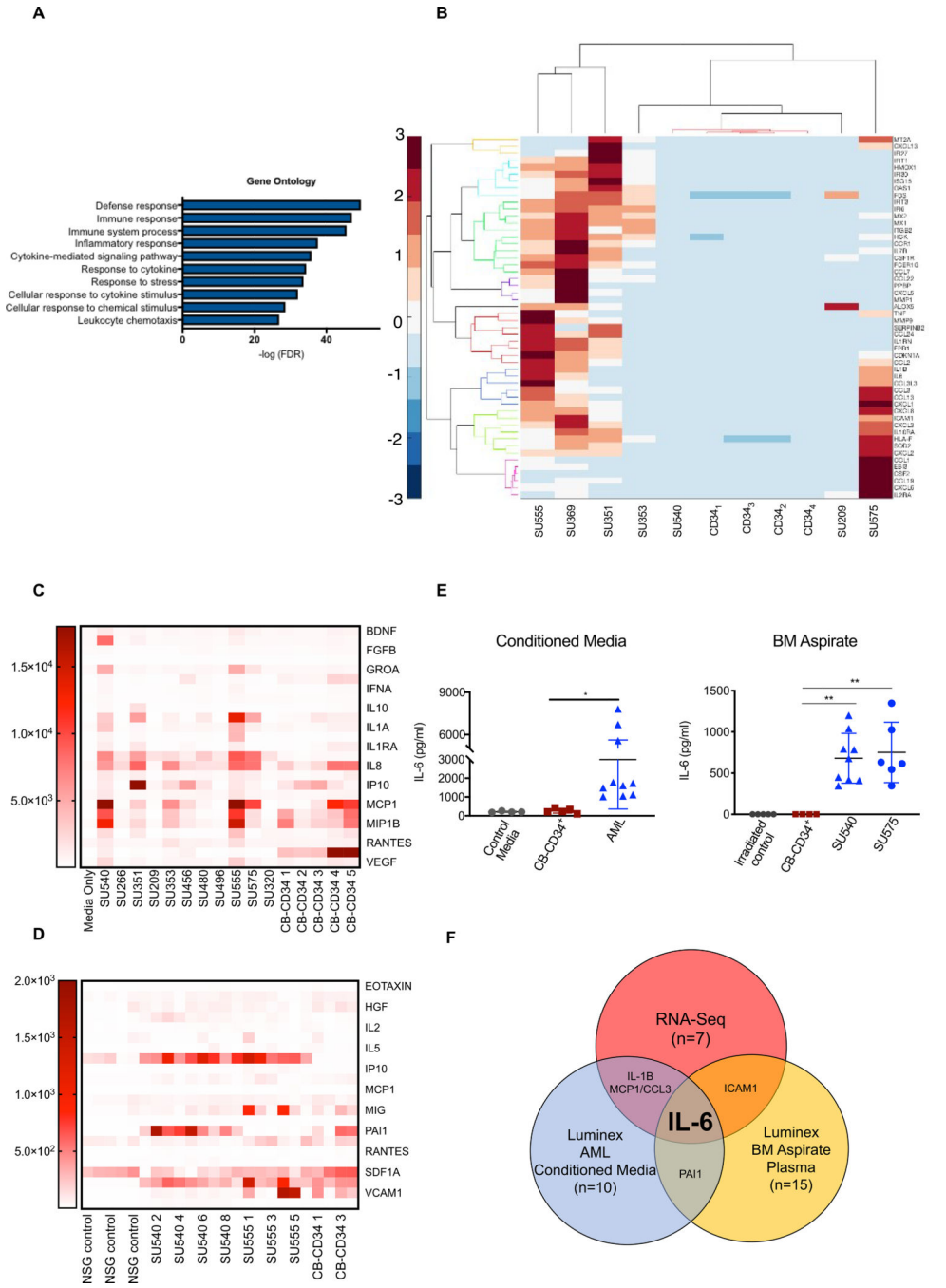

Fig. 6. IL-6 is differentially upregulated and secreted by AML blasts

(A) Gene ontology analysis of differentially upregulated transcripts in primary AML blasts (n=7) compared to normal human CB-CD34$^+$ cells (n=4), ranked by p-value. (B) Heatmap illustrating the expression pattern of genes upregulated (>=8 fold, p<0.0005) in primary AML compared to CB-CD34$^+$ cells associated with cytokines and/or cytokine signaling. (C) Heatmap summary of Luminex data showing expression of upregulated factors secreted by purified AML blasts in culture (n=10) compared to control media (n=3) and purified normal human CB-CD34$^+$ cells (n=5). (D) Heatmap summary of Luminex data showing upregulated

secreted factors in the BM plasma of NSG^{spln-}-PDX mice engrafted with SU540 (n=9) and SU555 (n=6) compared to irradiated only NSG^{spln-} mice (n=5) or NSG^{spln-}-CB-CD34^{+} mice (n=4). (E) Concentrations of IL-6 produced in individual experimental replicates reported in (C) and (D) $p<0.001$ (F) Schematic showing identification of IL-6 as a secreted factor upregulated by human AML blasts in all three platforms of evaluation.

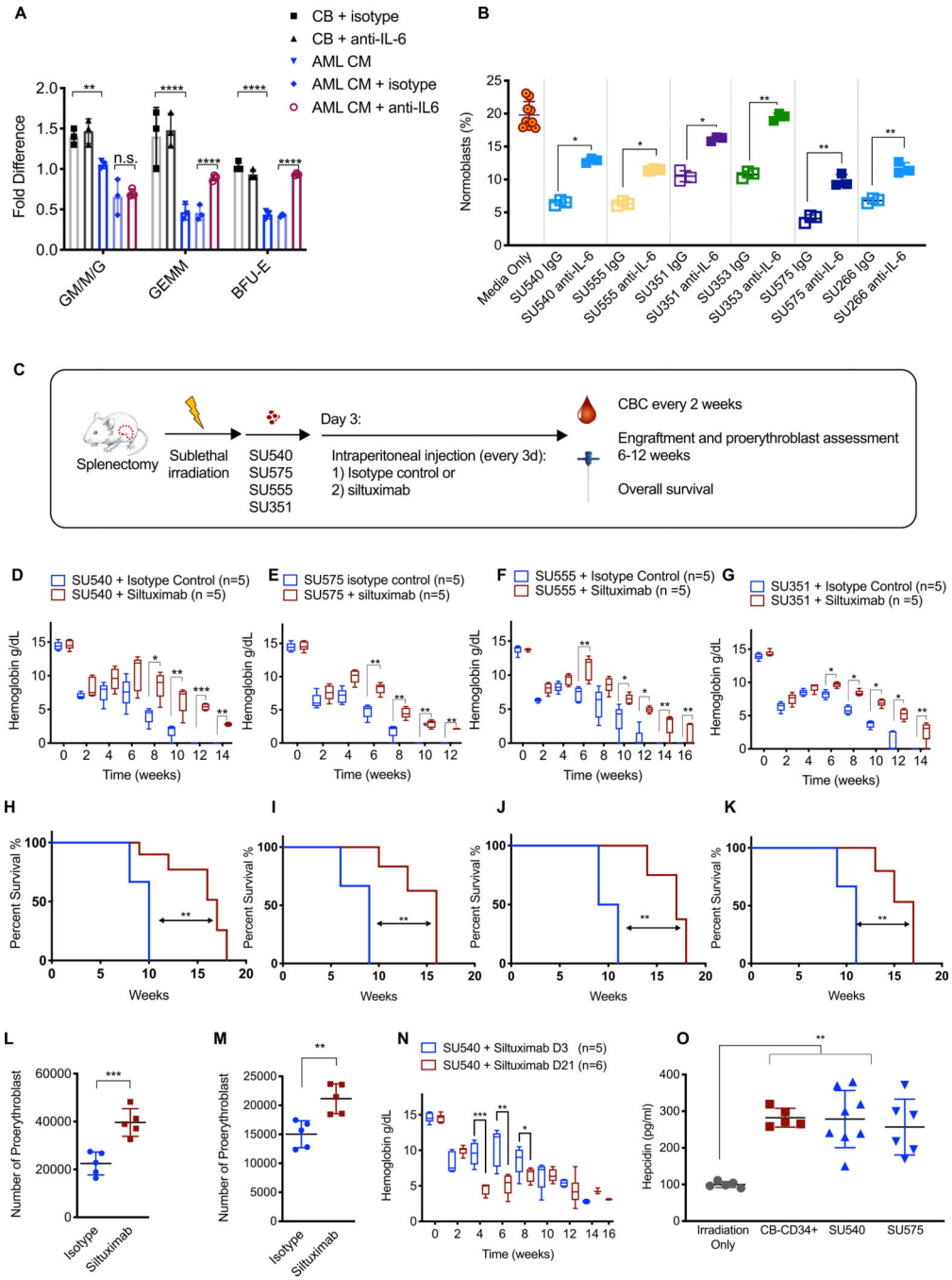

Fig. 7. Human AML suppresses erythroid differentiation and causes anemia via paracrine effects of IL-6

(A). Fold change in the number of colonies generated by normal human CB-CD34$^+$ cells in the presence of CB-CD34$^+$-CM (n=3) or human AML-CM (n=3) +/− human IL-6 neutralizing antibody or an isotype control antibody. The number of colonies was normalized to either CB-isotype control or AML-CM isotype controls as indicated by brackets in the figure. (B). Transwell assay for erythroid differentiation was done in the presence or absence of a human IL-6 neutralizing antibody or an isotype control antibody. Aliquot of cells from the top compartment was analyzed for the percentage of CD71$^+$GPA$^+$

normoblasts on day 6. (C). Schematic of experimental procedure. Treatment with control antibody or siltuximab (anti-human IL-6, 20 mg/kg) began on day 3 and occurred every 3 days. Hemoglobin in NSG^{spln-} mice engrafted with primary AML (D) SU540, (E) SU575, (F) SU555, and (G) SU351. Overall survival in NSG^{spln-}-PDX mice engrafted with (H) SU540 10 weeks vs 17 weeks p=0.02, (I) SU575 9 weeks vs 16 weeks, p=0.002, (J) SU555 10 weeks vs 17 weeks p=0.0014, and (K) SU351 11 weeks vs 16 weeks, p=0.006). Absolute numbers of $CD71^{+/}GPA^{+}$ normoblasts in NSG^{spln-}-PDX mice engrafted with (L) SU555 2.25×10^4 vs 3.96×10^4 p=0.0009 and (M) SU351 1.50×10^4 vs 2.11×10^4 p=0.004. (N) Hemoglobin in NSG^{spln-}-SU540 mice which began treatment on d3 versus d21. (O) Serum hepcidin concentrations in control, NSG^{spln-}-PDX engrafted with SU540 or SU575, and NSG^{spln-}-CB-$CD34^{+}$ mice (n=5 for each group, p=0.001). *P < 0.05, **P < 0.01, ***P < 0.001